Article

Temperature-Dependent Coordination in *E. coli* Manganese Superoxide Dismutase

Leandro C. Tabares, Nstor Cortez, Ileana Agalidis, and Sun Un

J. Am. Chem. Soc., **2005**, 127 (16), 6039-6047• DOI: 10.1021/ja047007r • Publication Date (Web): 29 March 2005

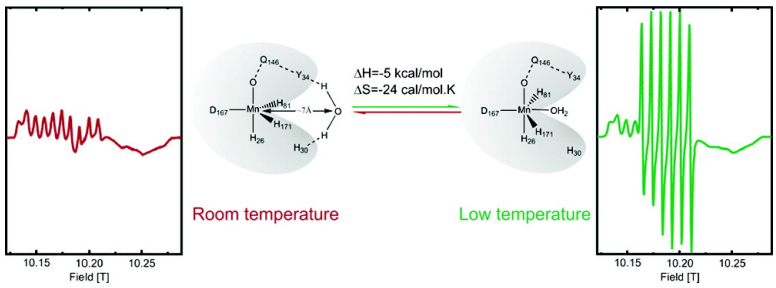

More About This Article

Additional resources and features associated with this article are available within the HTML version:

- Supporting Information
- Links to the 6 articles that cite this article, as of the time of this article download
- Access to high resolution figures
- Links to articles and content related to this article
- Copyright permission to reproduce figures and/or text from this article

View the Full Text HTML

J|A|C|S
ARTICLES
Published on Web 03/29/2005

Temperature-Dependent Coordination in *E. coli* Manganese Superoxide Dismutase

Leandro C. Tabares,[†,‡] Néstor Cortez,[‡] Ileana Agalidis,[§] and Sun Un*[,†]

Contribution from the Service de Bioénergétique, DBJC, CNRS URA 2096, CEA Saclay, 91191 Gif-sur-Yvette, France, Centre de Génétique Moléculaire, CNRS, 91198 Gif-sur-Yvette, France, and Instituto de Biología Molecular y Celular de Rosario (IBR), Universidad Nacional de Rosario and CONICET, Suipacha 531, S2002LRK Rosario, Argentina

Received May 21, 2004; E-mail: sun@ozias.saclay.cea.fr

Abstract: Two different temperature dependences of the manganese(II) high-field electron paramagnetic resonance spectrum of manganese superoxide dismutase from *E. coli* were observed. In the 25−200 K range, the zero-field interaction steadily decreased with increasing temperature. This was likely due to the thermal expansion of the protein. From these results, it was possible to deduce an approximately $r^{-2.5}$ dependence of Mn(II) zero-field interaction on ligand−metal distance. At temperatures above 240 K, a distinct six-line component was detected, the amplitude of which decreased with increasing temperature. On the basis of similarities to the six-line spectrum observed for the azide-complexed *E. coli* manganese superoxide dismutase, the newly detected six-line spectrum was assigned to a hexacoordinate Mn(II) center resulting from the coordination of a nearby water molecule to the normally five-coordinate center. The changes in enthalpy and entropy characterizing the hexacoordinate−pentacoordinate equilibrium in the 240−268 K range were −5 kcal/mol and −24 cal/mol·K, respectively. The structural implications of the zero-field parameters of the newly found hexacoordinate form in comparison to those of the Mn(II) centers in concanavalin-A and manganese-containing *R. spheroides* photosynthetic reaction centers and the values predicted by the superposition model are discussed.

Introduction

Superoxide dismutases (SOD) are enzymes that play a key role in cellular protection against oxidative stress conditions. They catalyze the disproportionation of superoxide ($O_2^{\bullet-}$) to form dioxygen and hydrogen peroxide[1,2] through a cyclic oxidation−reduction mechanism between the $O_2^{\bullet-}$ and the metal cofactor.[3−5] Four classes of SODs have been found and classified according to their native metal ion: manganese, iron, copper−zinc, and nickel.[1,6,7] The FeSOD and MnSODs are evolutionarily related, whereas the binuclear Cu/Zn and Ni enzymes belong to different lineages.[2]

Although there is a high degree of structural homology among the Fe−Mn family,[8−11] the activity is highly metal-specific[12,13] and only a small subgroup called cambialistic−SOD shows activity with both cofactors.[14−18] Within the Fe−Mn SOD family, the metal cofactor is coordinated by two histidines and an aspartic acid in the equatorial plane and a histidine and a solvent molecule (H_2O or HO^-) in the axial positions (Figure 1),[8,9] forming an unusual trigonal bipyramidal geometry.

Despite the high structural homology among Mn and FeSODs, it is possible to distinguish these enzymes based on their Mn(II) high-field electron paramagnetic resonance (HFEPR) spectra. The Mn(II) zero-field *D* and *E* parameters that determine the HFEPR Mn(II)SOD spectra are very sensitive to metal−protein interactions.[19] In general, the Mn(II, $S = {}^5/_2$) EPR spectra

[†] Service de Bioénergétique.
[‡] IBR, Universidad Nacional de Rosario and CONICET.
[§] Centre de Génétique Moléculaire.

(1) Fridovich, I. *Annu. Rev. Biochem.* **1995**, *64*, 97−112.
(2) Touati, D. In *Oxidative Stress and the Molecular Biology of Antioxidant Defenses*; Scandalios, J. G., Ed.; Cold Spring Harbor Press: New York, 1997; pp 447−493.
(3) Bull, C.; Fee, J. A. *J. Am. Chem. Soc.* **1985**, *107*, 3295−3304.
(4) Lavelle, F.; McAdam, M. E.; Fielden, E. M.; Roberts, P. B. *Biochem. J.* **1977**, *161*, 3−11.
(5) Klug-Roth, D.; Fridovich, I.; Rabani, J. *J. Am. Chem. Soc.* **1973**, *95*, 2786−2790.
(6) Kim, E. J.; Chung, H. J.; Suh, B.; Hah, Y. C.; Roe, J. H. *Mol. Microbiol.* **1998**, *27*, 187−195.
(7) Kim, F. J.; Kim, H. P.; Hah, Y. C.; Roe, J. H. *Eur. J. Biochem.* **1996**, *241*, 178−185.
(8) Stroupe, M. E.; DiDonato, M.; Tainer, J. A. In *Handbook of Metalloproteins*; Messerschmidt, A., Huber, R., Wieghardt, K., Paulos, T., Eds.; Wiley and Sons: Chichester, U.K., 2001; Vol. 2, pp 941−951.
(9) Miller, A.-F. In *Handbook of Metalloproteins*; Messerschmidt, A., Huber, R., Wieghardt, K., Paulos, T., Eds.; Wiley and Sons: Chichester, U.K., 2001; Vol. 1, pp 668−682.
(10) Schmidt, M.; Meier, B.; Parak, F. *J. Biol. Inorg. Chem.* **1996**, *1*, 532−541.
(11) Sugio, S.; Hiraoka, B. Y.; Yamakura, F. *Eur. J. Biochem.* **2000**, *267*, 3487−3495.
(12) Ose, D. E.; Fridovich, I. *J. Biol. Chem.* **1976**, *251*, 1217−1218.
(13) Hiraoka, B. Y.; Yamakura, F.; Sugio, S.; Nakayama, K. *Biochem. J.* **2000**, *345* (Part 2), 345−350.
(14) Meier, B.; Barra, D.; Bossa, F.; Calabrese, L.; Rotilio, G. *J. Biol. Chem.* **1982**, *257*, 13977−13980.
(15) Amano, A.; Shizukuishi, S.; Tamagawa, H.; Iwakura, K.; Tsunasawa, S.; Tsunemitsu, A. *J. Bacteriol.* **1990**, *172*, 1457−1463.
(16) Martin, M. E.; Byers, E. B. R.; Olson, M. O. J.; Salin, M. L.; Arceneaux, J. E. L.; Tolbert, C. *J. Biol. Chem.* **1986**, *261*, 9361−9367.
(17) Gregory, E. M. *Arch. Biochem. Biophys.* **1985**, *238*, 83−89.
(18) Tabares, L. C.; Bittel, C.; Carrillo, N.; Bortolotti, A.; Cortez, N. *J. Bacteriol.* **2003**, *185*, 3223−3227.
(19) Un, S.; Tabares, L. C.; Cortez, N.; Hiraoka, B. Y.; Yamakura, F. *J. Am. Chem. Soc.* **2004**, *126*, 2720−2726.

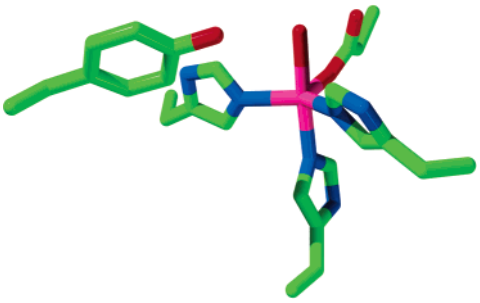

Figure 1. Structure of the EcMnSOD active site. The Mn ion is coordinated by an Asp and two His in the equatorial plane and another His and a solvent molecule in the axial positions. Tyr34, which is part the access channel, is shown.

are determined by the spin Hamiltonian

$$H = \beta\vec{B}\cdot\mathbf{g}\cdot\vec{S} + \vec{I}\cdot\mathbf{A}\cdot\vec{S} + \frac{D}{3}(3S_z^2 - S(S+1)) + \frac{E}{2}(S_+^2 - S_-^2) \quad (1)$$

where the first term describes the electronic Zeeman interaction and the second the hyperfine interaction between the unpaired electrons and the manganese nucleus ($I = {}^5/_2$). The last two terms describe the zero-field interaction. For Mn(II) ions in SOD, the Zeeman and hyperfine interactions are essentially isotropic, that is, they have no dependence on the orientation of the magnetic field, while the zero-field interaction is inherently anisotropic.

A detailed analysis of the HFEPR Mn(II)SOD spectra with respect to eq 1 has been previously presented.[19] For a Mn(II) ion, there are six electronic spin states, each of which is composed of six nuclear spin sublevels. At high magnetic fields, such as those used in our experiments, the electronic Zeeman interaction dominates and the electronic spin levels are well separated according to their Zeeman energies. The transitions between $M_s = -{}^1/_2$ and $M_s = +{}^1/_2$ electron-spin manifolds are unaffected by the zero-field interaction to first order and are the only ones detected in our HFEPR experiments. By contrast, the transitions between the other electron-spin manifolds depend directly on the zero-field interaction, and in frozen solution samples, where the protein molecules are randomly orientated, the resonances corresponding to these transitions are extremely broad and are difficult to detect due to their dependence on the orientation of the zero-field interaction. The complex shape of the SOD spectra of the type shown in Figure 2 is due to the second-order contribution of the zero-field interaction and the much smaller hyperfine interaction. The partially resolved fine structure is due to transitions between the nuclear hyperfine sublevels of the $M_s = -{}^1/_2$ and $M_s = +{}^1/_2$ electron-spin manifolds. There are six formally allowed nuclear hyperfine transitions between these two states that leave the nuclear spin state unchanged ($\Delta m_I = 0$) and a number of formally forbidden transitions that involve the simultaneous change in the electronic and nuclear spin state. The resonant field positions of these forbidden transitions lie between the allowed ones. The amplitudes of the forbidden transitions relative to the allowed ones depend on the orientation of the magnetic field and the square of the ratio of the zero-field and Zeeman interactions. For orientations corresponding to the lower half of the Mn(II)SOD spectrum, the amplitude of the forbidden transitions is close to zero. By contrast, the upper half of the spectrum corresponds

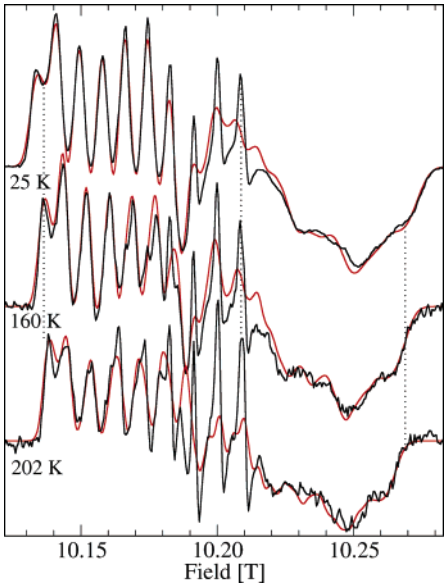

Figure 2. The 285 GHz Mn(II) spectra of EcMnSOD as a function of temperature, observed (black) and simulation (red).

to field orientations where the forbidden transition amplitudes rival those of the allowed. It is for this reason that the Mn(II)SOD spectra look more resolved at the low-field edge and much less so at the high-field edge. When the second-order zero-field contribution is smaller than the hyperfine interaction, one expects narrower resonances and a sharp decrease in the amplitude of the forbidden transitions, resulting in a spectrum composed of six relatively sharp lines. In this case, the lines would be evenly spaced by the hyperfine coupling constant. This is the case for the HFEPR spectra of azide−Mn(II)SOD complexes.[20]

In our previous work, we determined the magnetic spin parameters of several different SODs using HFEPR and demonstrated the high sensitivity of this technique to a small variation in Mn(II) centers.[19] In this paper, the temperature dependence of the Mn(II) zero-field interaction in EcMn(II)SOD and EcMn(II)(Fe)SOD and its implications on the structure of the Mn(II) bonding site are examined. We also showed that the metal ion in EcMn(II)SOD undergoes a change from penta- to hexacoordinate at temperatures well below 0 °C.

Experimental Section

Samples. *Escherichia coli* Mn- and FeSODs and concanavalin-A were purchased from commercial sources (Sigma-Aldrich). The SODs were washed several times with 0.1 mM EDTA in 10 mM pH 7.8 Tris buffer to remove any adventitious manganese ions. The final concentration was 0.4 mM active sites. Manganese(II) substitution into *E. coli* FeSOD is described in reference 19. Biosynthetic manganese enrichment was performed on *Rhodobacter spheroides* Y cells grown photosynthetically, and the reaction centers were purified as described in reference 21. All spectra were obtained with 10 G modulation under nonsaturating conditions at 25 K, unless otherwise noted and with 5 G resolution.

Simulations. Simulations of the HFEPR spectra were carried out in a manner similar to those previously described using a spin Hamiltonian with isotropic Zeeman and hyperfine interactions and D and E terms

(20) Un, S.; Dorlet, P.; Voyard, G.; Tabares, L. C.; Cortez, N. *J. Am. Chem. Soc.* **2001**, *123*, 10123−10124.
(21) Rutherford, A. W.; Agalidis, I.; Reiss-Husson, F. *FEBS Lett.* **1985**, *182*, 151−157.

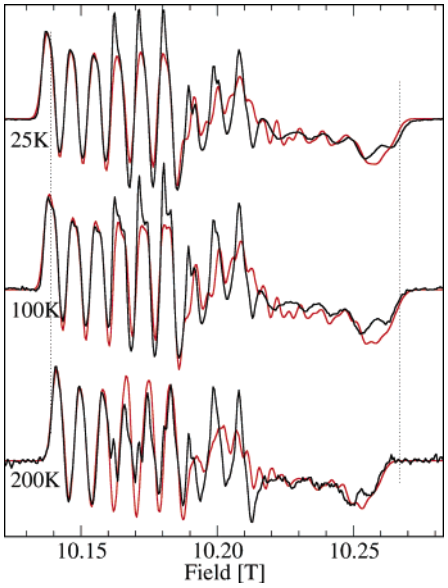

Figure 3. The 285 GHz Mn(II) spectra of EcMn(Fe)SOD as a function of temperature, observed (black) and simulation (red).

of the zero-field interaction.[19] The transition energies could be calculated to good accuracy using third-order perturbation theory approximation of the energies. However, a complete diagonalization of the spin Hamiltonian was used to obtain the eigenfunctions required to calculate transition probabilities. This was a computationally expensive step. Since then, we have become aware that Bir[22] had derived second-order perturbation approximations for the transition probabilities. By comparing the results to the diagonalization method, Bir's method was established to be as accurate. The increased computational efficiency allowed us to incorporate the effect of distributions in the zero-field parameters. Kliava[23] has discussed this issue in detail. In our calculations, we chose to take the simplest model, where the distribution in D and E were gaussian and statistically independent of each other. The estimated errors in the zero-field parameters were ± 0.050 GHz. In all cases, the simulations were normalized to the observed spectra using linear regression to obtain the best fit. In the temperature studies shown in Figures 2 and 3, no attempt was made to fit the spectra as a function of temperature. Over such a broad temperature range, the microwave transmission properties of the sample change significantly and make it difficult to obtain amplitudes that can be meaningfully compared over the total range.

Quantum Chemical Calculations. Hybrid Hartree−Fock density functional calculations were performed with Gaussian94.[24] Geometry optimization and subsequent thermochemical analysis were carried out using the B3LYP density functional and correlation function and the 6-31+G(D,P) basis set. The calculations were carried out in vacuum and in solvent environments with dielectric constants of 4 and 10 D to simulate the protein environment. The latter were carried out using the Onsager reaction field model as implemented in Gaussian94.

Linear regression and power-law fits were carried using the plotting program Xmgrace (information about the program may be obtained from http://plasma-gate.weizmann.ac.il/Grace/).

(22) Bir, G. L. *Sov. Phys. Solid State* **1964**, *5*, 1628−1635.
(23) Kliava, J. *Phys. Status Solidi B* **1986**, *134*, 411−455.
(24) Frisch, M. J.; Trucks, G. W.; Schlegel, H. B.; Gill, P. M. W.; Johnson, B. G.; Robb, M. A.; Cheeseman, J. R.; Keith, T.; Petersson, G. A.; Montgomery, J. A.; Raghavachari, K.; Al-Laham, M. A.; Zakrzewski, V. G.; Ortiz, J. V.; Foresman, J. B.; Cioslowski, J.; Stefanov, B. B.; Nanayakkara, A.; Challacombe, M.; Peng, C. Y.; Ayala, P. Y.; Chen, W.; Wong, M. W.; Andres, J. L.; Replogle, E. S.; Gomperts, R.; Martin, R. L.; Fox, D. J.; Binkley, J. S.; Defrees, D. J.; Baker, J.; Stewart, J. P.; Head-Gordon, M.; Gonzalez, C.; Pople, J. A. *Gaussian94*; Gaussian, Inc.: Pittsburgh, PA, 1995.

Results

The temperature dependence of the 285 GHz HFEPR spectra of MnSOD from *Escherichia coli* (EcMnSOD) is shown in Figure 2 along with the simulations of each of the spectra (Table 1). The Bir-based simulation of the spectra that also incorporated distributed zero-field parameters gave improved simulations over those previously reported.[19] This better agreement was a direct result of using gaussian distributions for both $|D|$ and E ranging from 0.175 to 0.220 GHz for former and 0.180 to 0.230 for the latter (see Supporting Information for details). The main visual effect of the gaussian distribution was to broaden the fine structure on the high-field half of the simulated spectra (for example, see ref 19), leading to better agreement with the experimental data. This asymmetric effect of the distribution on the spectra appears to be a consequence of the resonances corresponding to the formally forbidden transitions that have maximum amplitude at the high-field end of the spectrum and vanish at the low-field end. The resonant field positions of the forbidden transitions, like those of the allowed, directly depend on the two zero-field parameters, and any distribution in these values will lead directly to broadened resonances. For this reason, the high-field half of the spectra, which has intensity from both allowed and forbidden transitions, is more affected by a spread in the $|D|$ and E values than the low-field half. It is important to note that the improved simulations did not lead to significantly different $|D|$ and E values from those previously reported. This was not unexpected since the multifrequency approach in the previous study strongly constrained the simulations.[19]

The most notable trend was that the extent of the EcMnSOD spectrum decreased with increasing temperature (Figure 2). The simulations showed that this decrease resulted from a decrease in the zero-field $|D|$ value (Figure 4) and possibly the E parameter. The overall decrease in E was slightly larger than the estimated error of the fitting procedure. Within this uncertainty, the E/D ratio of 0.081 was essentially independent of temperature (Figure 4, top). The temperature dependence could be fit to a $T^{-2.6}$ inverse power law with an asymptotic zero-temperature $|D|$ value of 10.630 GHz (Figure 4, bottom).

Similar temperature dependence was also observed for the Mn(II)-substituted *E. coli* iron SOD (EcMn(Fe)SOD) (Figure 3). In this case, inclusion of distributed zero-field parameters, with a distribution in $|D|$ ranging from 0.099 to 0.150 GHz and in E from 0.120 to 0.180 GHz (see Supporting Information for details), led to only slight improvements in the fits, and overall, the fits were not as good as those of the EcMn(II)SOD spectra. As was the case with the EcMnSOD protein, the 25 K zero-field parameters did not significantly differ from those previously reported. The agreement between simulation and experiment was nearly exact at the low-field edge of the EcMn(II)(Fe)-SOD spectrum, while simulated shape of the high-field edge differed from the experiment. Since the low-field edge is defined by the sum of the two zero-field parameters,[19] it was concluded that while the $|D|$ and E values obtained from the fits must closely correspond to the "average" values for the Mn(II) ion in EcMn(Fe)SOD, the variation in these zero-field parameters, unlike in the case of the EcMnSOD, could not be adequately modeled by simple gaussians. For this reason, we consider that the reported values (Table 1) reliably reflect the average $|D|$ and E parameters. The temperature dependence of $|D|$ and

Table 1. Experimentally Determined and SP Model Predicted Zero-Field $|D|$ and E Values of Various Mn(II) Centers[a]

Mn(II) center	$\|D\|$ (GHz)	E (GHz)	L–Mn(II)–L Angle smallest	L–Mn(II)–L Angle largest	PDB Code	Superposition Model D (GHZ)	Superposition Model E (GHZ)	Superposition Model orientation
concanavalin-A	0.875	0.289	82	173	1NLS	0.87	0.24	within 15° of single crystal study
EcMnSOD + azide	1.386	0.273	75	171	1MNG	−1.40	0.27	along His−Mn−OH bond
EcMnSOD, 240 K	1.443	0.275	83	172	1D5N	−1.44	0.26	along Asp−Mn−Water bond
Mn(II), *R. spheroides*	3.328	0.749	60	142	1YST			none found
Mn(II) in $[Cd(bispicam)_2]^{2+}$ [b]	5.25	0.0	71−74	148−150	KUTMUH[c] KUTNAO[c]			none found
EcMnSOD[d], 25 K	10.640	0.853	107[e]	176[e]	1VEW			
EcMnSOD[d], 202 K	9.766	0.778						
EcMn(Fe)SOD[d,f], 25 K	10.521	0.381						
EcMn(Fe)SOD[d,f], 202 K	9.950	0.408						

[a] Smallest and largest ligand−metal−ligand angles are a measure of the asymmetry of the Mn(II) binding site. Descriptions of the zero-field axis orientation for which the SP model and experimental values matched are also given. [b] Bis(2-pyridylmethyl)amine complex of Cd(II). [c] Cambridge Structure Database accession code. [d] No superposition model calculations were carried out for the pentacoordinate center (see text for details). [e] Smallest angle in the equatorial plane and the largest angle bond is the angle formed by the axial ligands in the trigonal bipyramidal structure. [f] Crystallographic structure has not been determined.

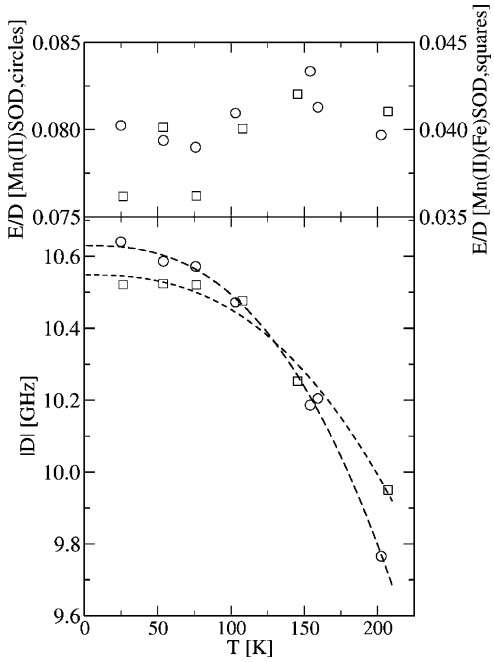

Figure 4. Temperature dependence of the zero-field parameter $|D|$ (bottom) and the relationship of E/D (top) for the EcMnSOD (circles) and EcMn(Fe)SOD (squares).

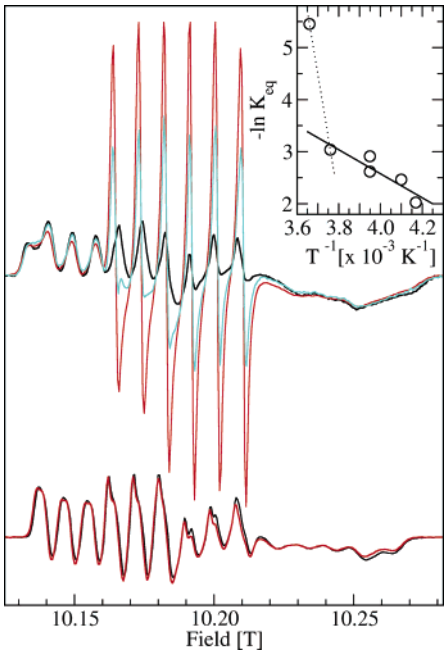

Figure 5. Upper: The 285 GHz at 25 K HFEPR spectra of EcMnSOD after incubation at 298 (black), 266 (blue), and 240 K (red). Lower: The 285 GHz at 25 K HFEPR spectra of EcMn(Fe)SOD after incubation at 285 (black) and 240 K (red). Inset: van't Hoff plot of the equilibrium constant between five- and six-coordinated EcMnSOD. The thermodynamic parameters were obtained by linear fitting of the data points below 270 K.

E/D are shown in Figure 4. The temperature dependence of the EcMn(Fe)SOD $|D|$ value was characterized by a $T^{-2.5}$ dependence. The power fits were not as a good as in the case of EcMn(II)SOD, probably due to our inability to exactly describe the distribution in the zero-field values.

At temperatures above 240 K, a more striking change in the HFEPR spectra of the EcMnSOD was observed, the appearance of a sharp six-line component (Figure 5, top). The high-temperature spectra were reminiscent of the EcMnSOD−azide complex spectrum.[20] Azide binding leads to a hexacoordinate manganese center with a near octahedral geometry[25] and a sharp decrease in the zero-field parameters resulting in a sharp six-line spectrum. On the basis of the similarity of the six-line components, the newly found 240 K component was assigned to a hexacoordinate Mn(II) center. The same six-line spectrum detected at 240 K could also be observed at 25 K by first incubating the sample at 240 K and flash-freezing in liquid nitrogen. Melting such an incubated sample and reflash-freezing resulted in the disappearance of the six-line component. Hence, the formation of the hexacoordinate Mn(II) center was completely reversible and did not involve release of Mn(II). Under identical conditions, the EcMn(Fe)SOD protein, which is known to be inactive,[12,13] exhibited no evidence of a six-line spectrum (Figure 5).

The spin parameters of the 240 K six-line component were obtained by fitting the HFEPR spectra taken at three different frequencies (Figure 6). Simultaneous multifrequency fitting was necessary since the zero-field contribution was essentially to the width of each of the six lines and to the subtle asymmetric effects on the line shape. The $|D|$ and E values were determined to be 1.443 and 0.275 GHz, respectively (Table 1). These values were very similar to those of the EcMnSOD−azide complex

(25) Lah, M. S.; Dixon, M. M.; Pattridge, K. A.; Stallings, W. C.; Fee, J. A.; Ludwig, M. L. *Biochemistry* **1995**, *34*, 1646−1660.

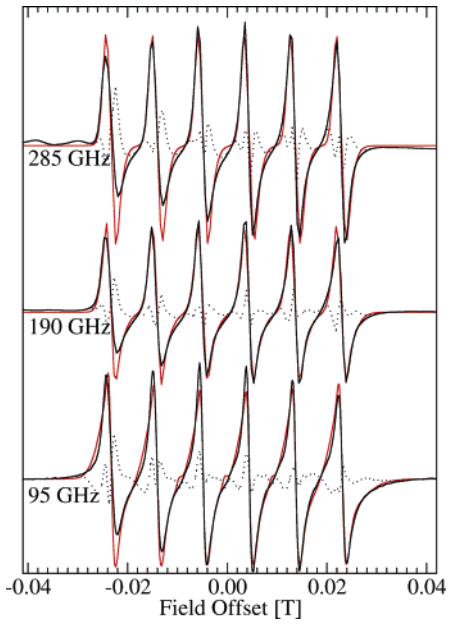

Figure 6. Six-line portion of the 285 (top), 190 (center), and 95 GHz (bottom) HFEPR EcMnSOD spectra after 240 K incubation (black) and simulations (red) obtained from the simultaneous fit of the three spectra. The differences between the observed and simulation are also shown (dotted lines).

(Table 1). Relatively large distributions of 0.950 GHz for $|D|$ and 0.184 GHz for E were required to account for the broad tails that were especially apparent on the last (highest-field) hyperfine line of the 95 GHz spectrum. Some, but not all, of the discrepancies between the simulations and experimental data were probably due to the presence of the underlying broader resonances arising from the pentacoordinate centers. For each observation frequency, the difference in amplitude between simulation and experiment was systematic, decreasing with increasing magnetic field. This would occur if the observed spectra had contributions from centers which possessed $|D|$ values that were larger than could be accounted for by our simple gaussian distribution model.

Between 240 and 273 K, the six-line component increased in intensity with decreasing incubation temperature (Figure 5). The kinetics of this five to six ligand change was also clearly temperature dependent. Although at room temperature no incubation time was required, it took at least 24 h to reach equilibrium at 240 K. Below 200 K, no changes in the six-line intensity were observed, even after many days, indicating extremely slow kinetics or a threshold temperature for the transition. The intensity of the six lines did not appear to change in the pH range between 7.2 and 8.8 (data not shown). Since the five- and six-coordinated species could be readily resolved, a thermodynamic analysis of the equilibrium between these two states was possible. The spectra of the samples incubated between 240 and 273 K were decomposed by subtracting a scaled version of the 25 K spectrum of the sample incubated at 293 K, which contained no narrow six-line component. The difference spectra, which contained only the six-line component, were doubly integrated to obtain the relative concentration of hexacoordinate centers. For the pentacoordinate centers, the concentration was obtained from the product of the scaling factor required for the subtraction and the double integral of the 25 K spectrum of the sample incubated at 298 K. The amount of six-line component in the sample incubated at 273 K was 2-fold larger than the estimated error of the procedure. The van't Hoff plot (Figure 5, inset) was reasonably linear from 240 to 268 K, but showed a strong break (dotted line) just below 273 K, suggesting that above the melting point, other equilibria were involved. Linear regression analysis over 240−269 K yielded $\Delta H = -5 \pm 1$ kcal/mol and $\Delta S = -24 \pm 5$ cal/mol·K (solid line).

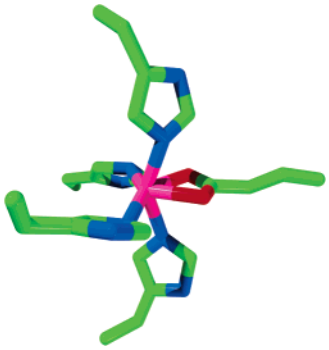

Figure 7. Structure of the metal binding site in manganese-containing the *R. spheroides* photosynthetic reaction centers showing the bidentate Glu and the four coordinating histidines.

To better understand the relationship between the geometry of the hexacoordinate Mn(II) binding site and the magnitude of the zero-field interaction, we also examined two very different metal sites, the highly distorted one in the manganese-containing photosynthetic reaction center in *R. spheroides* and the nearly trigonally distorted octahedral site in concanavalin-A. The former, which has a bidentate glutamate ligand, was used to address the question of whether it was likely that the aspartate ligand in EcMnSOD became bidentate at low temperatures. This had been previously suggested as a possibility for the low-temperature hexacoordinate EcMn(III)SOD site observed in the presence of azide.[26] The Mn(II) site in the *R. spheroides* photosynthetic reaction is composed of four histidines and a bidentate glutamate with the smallest ligand−metal−ligand angle of 60° and the largest only 142° (Figure 7, Table 1).[27] The 285 and 190 GHz HFEPR spectrum is shown in Figure 8. HFEPR spectra of this protein sample also had a small contribution from adventitious Mn(II) ions. The spectra of the Mn(II)-containing reaction centers were composed of six lines, each of which had partially resolved structure. For a given microwave frequency, the broadening increased with each subsequent hyperfine line (going from low to high field). This contribution was also larger at 190 than at 285 GHz. These observations were entirely consistent with electronic spin transitions between the $M_s = -1/2$ and $M_s = +1/2$ manifolds for which the second-order zero-field contribution is slightly smaller than the hyperfine interaction. The Mn(II) HFEPR spectra of the reaction centers were clearly different from the newly detected six-line EcMnSOD spectra. Simultaneous fit of the reaction center data yielded $|D|$ and E values of 3.328 and 0.749 (Table 1), respectively, with distributions of 0.130 and 0.250 GHz.

The Mn(II) binding site in concanavalin-A possesses a near ideal octahedral symmetry (Table 1).[28] The spectra exhibited

(26) Whittaker, M. M.; Whittaker, J. W. *Biochemistry* **1996**, *35*, 6762−6770.
(27) Arnoux, B.; Gaucher, J.-F.; Ducruix, A.; Reiss-Husson, F. *Acta Crystallogr. D* **1995**, *51*, 368−379.
(28) Deacon, A.; Gleichmann, T.; Kalb-Gilboa, A. J.; Price, H.; Raftery, J.; Bradbrook, G.; Yariv, J.; Helliwell, J. R. *J. Chem. Soc., Faraday Trans.* **1997**, *93*, 4305.

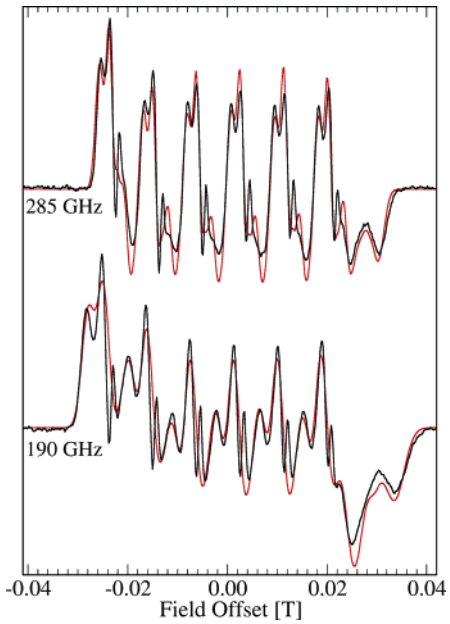

Figure 8. The 285 (top) and 190 GHz (bottom) Mn(II) HFEPR spectra of the manganese-containing *R. spheroides* photosynthetic reaction centers (black) and simulations (red) obtained from the simultaneous fit of both spectra.

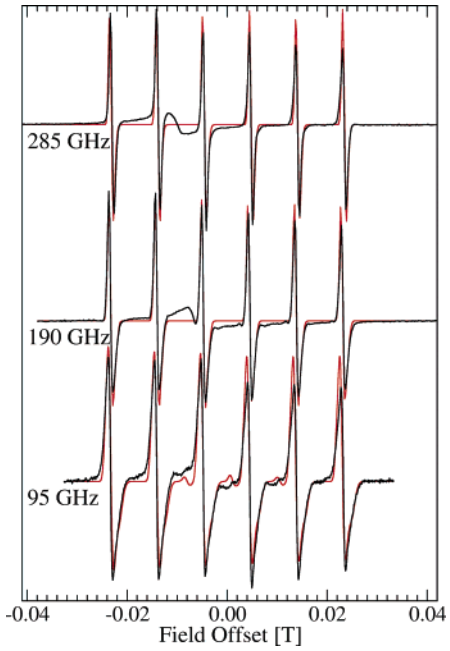

Figure 9. The 285 (top), 190 (center), and 95 GHz (bottom) Mn(II) HFEPR spectra of concanavalin-A (black) and simulations (red) obtained from the simultaneous fit of all three spectra.

six very sharp lines (Figure 9). There was a contribution from an unidentified broader component that appeared at three frequencies, underneath the second hyperfine resonance in the 285 GHz spectrum and the third in the 190 GHz spectrum. In the 95 GHz spectrum, there were weak resonances corresponding to the formally forbidden transition arising from the simultaneous excitation of the electron and nuclear spins. The simulation procedure accounted for both the position and relative amplitudes of these resonances. A comparison of Figures 6 and 9 shows that the line widths of the concanavalin-A hyperfine lines were smaller than those of EcMnSOD spectra, indicating a much smaller zero-field interaction. The $|D|$ and E values were found to be 0.875 and 0.289 GHz, respectively (Table 1), in reasonable agreement with the average of the two sites detected by previous HFEPR measurement on single crystals.[29] The $|D|$ value was the smallest of those examined in this study.

Discussion

The temperature dependence of the Mn(II) HFEPR spectra of SODs provides a number of insights into the nature of Mn(II) zero-field interaction and the structure of the MnSOD active site. At low temperatures (<200 K), the EcMnSOD $|D|$ value decreased with increasing temperature. Moreover, the E/D ratio remained largely constant in this temperature region, indicating that the overall symmetry of the ligand field was not temperature dependent. It has long been known that the zero-field interactions of Mn(II) ions in inorganic solids are pressure and temperature dependent due to their sensitivity to the metal−ligand distances.[30−34] For this reason, the simplest explanation for the changes that were observed at low temperatures (<200 K) was the thermal expansion of the protein. If this expansion is linear in temperature,[35] then the changes in Figure 2 correspond to a −2.5 power dependence of D on the Mn(II)−ligand distances. We cannot exclude the possibility that observed temperature dependences could have also been due to changes in the angular positions of the ligands or some combination of both angles and distances. The isotropic expansion model is appealing because it would preserve the symmetry of the manganese site consistent with a constant E/D ratio. There appears to be little data on the linear expansion coefficient of proteins at very low temperatures. The thermal expansion coefficient for metmyoglobin has been determined to be about 1.15×10^{-4} K^{-1} from 80 to 300 K,[35] about 1.2×10^{-4} K^{-1} from 95 to 295 K[36] for lysozyme, and at much higher temperatures for staphylococcal nuclease, about 8.9×10^{-4} K^{-1} from 288 to 308 K.[37] If one assumes a linear expansion coefficient for SODs of 10^{-4} K^{-1}, similar to those measured at low temperatures for the other proteins, then the variation in D (Figure 4) would correspond to changes in the average bond lengths of 0.04 Å. This implies that the difference of 0.1 GHz in the $|D|$ values of EcMnSOD and EcMn(Fe)SOD is due to differences in the structure of the Mn binding site that are on the order of a few hundredths of an angstrom, and that the structures of the binding sites of all of the other SODs thus far studied[19] are also within this range.

The more dramatic changes in the EcMnSOD spectra above 240 K (Figure 5) were clearly indicative of a much larger reduction in the zero-field interaction than that observed below 200 K. As noted above, the 240 K six-line spectrum closely resembles that of the azide−protein complex,[20] leading us to conclude that the appearance of the distinctive six-line component was due to a change from pentacoordination to hexa-

(29) Carmieli, R.; Manikandan, P.; Epel, B.; Kalb, A. J.; Schnegg, A.; Savitsky, A.; Mobius, K.; Goldfarb, D. *Biochemistry* **2003**, *42*, 7863−7870.
(30) Feher, E. *Phys. Rev.* **1964**, *136*, A145−A157.
(31) Sharma, R. R.; Das, T. P.; Orbach, R. *Phys. Rev.* **1968**, *171*, 378−388.
(32) Sharma, R. R. *Phys. Rev. B* **1970**, *2*, 3316−3318.
(33) Heming, M.; Remme, S.; Lehmann, G. *J. Magn. Reson.* **1986**, *69*, 134−143.
(34) Wen-Chen, Z. J. *Phys. Chem. Solids* **1993**, *54*, 1587−1592.
(35) Frauenfelder, H.; Hartmann, H.; Karplus, M.; Kuntz, I. D.; Kuriyan, J.; Parak, F.; Petsko, G. A.; Ringe, D.; Tilton, R. F.; Connolly, M. L.; Max, N. *Biochemistry* **1987**, *26*, 254−261.
(36) Kurinov, I. V.; Harrison, R. W. *Acta Crystallogr. D* **1995**, *51*, 98−109.
(37) Seemann, H.; Winter, R.; Royer, C. A. *J. Mol. Biol.* **2001**, *307*, 1091−1102.

coordination. Hexacoordination could occur if the aspartate ligand became bidentate at temperatures below freezing. This would presumably lead to a distorted octahedral site. For example, in the case of the metal site in the *R. spheroides* photosynthetic reaction centers, the oxygen−metal−oxygen bond angle of the bidentate glutamate ligand is 60°. The measured $|D|$ parameters for various Mn(II) binding sites, summarized in Table 1, argue against such an internal change to a bidentate aspartate ligand. The zero-field parameters of the 240 K six-line component are almost within error of the simulations of those measured for the EcMnSOD−azide complex. By comparison, highly distorted octahedral Mn(II) sites, such as those found in the *R. spheroides* reaction centers and Mn(II)-doped bis(2-pyridylmethyl)amine complexes of Zn(II) and Cd(II) reported by Glerup and co-workers,[38] have $|D|$ values that are much larger than that measured for the 240 K species (Table 1).

For six- and four-coordinate d^5 metal ions, the empirical superposition model (SPM) of Newman and Urban[39] has been successfully used to predict and rationalize both sign and magnitude of their zero-field parameters. The model is given by

$$b_2^m = \sum_i K_{2i}^m B_2(R_i) \qquad (2)$$

where b_2^0 is equal to D, and b_2^2, $3E$, and K_{2i}^m are well-known angular functions solely dependent on the polar angular coordinates of the ith ligand with respect to the zero-field axis system. The second term of the product in eq 2 is defined by

$$B_2(R_i) = B_2(R_0) \times \left(\frac{R_0}{R_i}\right)^t \qquad (3)$$

where $B_2(R_i)$ is specific to a ligand atom and is a function of the distance from that atom to the metal ion. The $B_2(R_0)$ is the reference value for the same type of ligand atom obtained at a ligand distance of R_0. For most common ligands, the $B_2(R_0)$ values have been determined.[33] The value of t is thought to be about 7.[40] If the structure of the Mn(II) binding site is known, then it is possible to predict the zero-field parameters for a given Mn(II) ion. Implicit in the usage of eq 2 is that the orientation of the zero-field axis system with respect to the molecular framework must also be known.

Equation 2 was applied to the different Mn(II) binding sites for which the structures are known. The site in concanavalin-A is essentially octahedral with a tetragonal elongation.[28] The MnSOD−azide complex is more distorted, but the bond angles do not deviate by more than 20° from ideal values. Equation 2 was calculated at 10° intervals for both polar angles upon which the K terms depend. In the case of concanavalin-A, the agreement between the experimental zero-field parameters and those predicted by SPM occurred when the polar angles were within 15° of those measured in a previous single crystal study (Table 1).[29] For the MnSOD−azide complex, good agreement was achieved for angles where the zero-field axis was within 10° of the His−Mn(II)−solvent direction. By contrast, no matter what zero-field axis orientation was assumed, the SPM D values for the *R. spheroides* reaction center and the Mn(II)-doped bis(2-pyridylmethyl)amine Cd(II) complex were much smaller than the experimental values, less than 1.4 GHz for the former and less than 0.3 GHz for the latter.

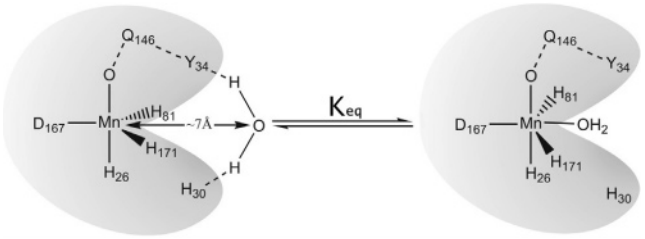

Figure 10. Schematic view of the EcMnSOD active site. Within the access channel, there are two water molecules about 7 Å from the manganese ion, one hydrogen bonds to Tyr34 and the other to His30 (in the drawing, both are represented by a single molecule). At temperatures below 273 K, a water molecule coordinates the manganese center, forming an octahedral center and results in a six-line HFEPR spectrum.

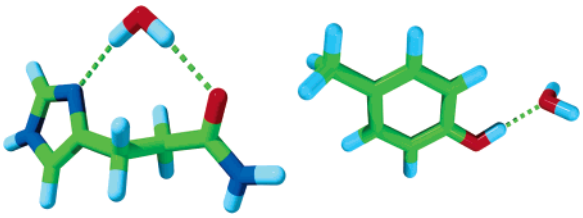

Figure 11. Optimized hydrogen-bonding structures of model tyrosine (right) and histidine water complexes (left). In the histidine model, the calculated distances from the water oxygen to the ring nitrogen and to the carbonyl oxygen were both 3.10 Å. In the tyrosine model, the oxygen−oxygen distance was 2.73 Å.

SPM values for the hexacoordinate EcMnSOD site obtained by rapid freezing of a single crystal[41] were also calculated. As explained below, we were unable to trap this state. Nonetheless, the structure of this state should serve as a good model of the 240 K hexacoordinate form that we were able to detect. In this case, good agreement between the experimentally determined and SPM-predicted zero-field values occurred for angles which required the zero-field axis to be directed approximately along the aspartate−Mn(II) bond and also the sixth ligand (Table 1). When the zero-field axis was assumed to be along the axial His−Mn(II)−solvent direction, as in the case of the azide complex, no reasonable values were found. Although it is not clear what the origin of this difference is, the SPM predictions were further evidence that the conversion from penta- to hexacoordination was due to a sixth ligand and a nearly octahedral coordination sphere rather than a highly distorted coordination arrangement involving a bidentate aspartate ligand.

The most likely candidate for the sixth ligand was one of the two waters located in the access channel[42,43] and close to the metal ion (Figure 10). A water ligand was favored over a hydroxide since a variation in hydroxide concentration by a factor of 40 (from pH 7.2 to 8.8) had no effect on the spectra. This also implied that the process was unlikely due to a pK_a effect. Of the two water molecules that were of interest, one is hydrogen-bonded to Tyr34 and the other to His30 (Figure 10).

(38) Glerup, J.; Goodson, P. A.; Hodgson, D. J.; Michelsen, K.; Nielsen, K. M.; Weihe, H. *Inorg. Chem.* **1992**, *31*, 4611−4616.
(39) Newman, D. J.; Urban, W. *Adv. Phys.* **1975**, *24*, 793−844.
(40) Newman, D. J.; Siegel, E. *J. Phys. C: Solid State Phys.* **1976**, *9*, 4285−4292.
(41) Borgstahl, G. E. O.; Pokross, M.; Chehab, R.; Sekher, A.; Snell, E. H. *J. Mol. Biol.* **2000**, *296*, 951−959.
(42) Edwards, R. A.; Baker, H. M.; Whittaker, M. M.; Whittaker, J. W.; Jameson, G. B.; Baker, E. N. *J. Biol. Chem.* **1998**, *3*, 161−171.
(43) Borgstahl, G. E.; Parge, H. E.; Hickey, M. J.; Beyer, W. F. J.; Hallewell, R. A.; Tainer, J. A. *Cell* **1992**, *71*, 107−118.

Table 2. Summary of Thermochemical Analysis of the Hydrogen Bonding between Water and Tyrosine and Histidine (see text for details)

	$\Delta H(\epsilon = 1)$ (kcal/mol)	$\Delta S(\epsilon = 1)$ (cal/mol·K)	$\Delta H(\epsilon = 4)$ (kcal/mol)	$\Delta S(\epsilon = 4)$ (cal/mol·K)	$\Delta H(\epsilon = 10)$ (kcal/mol)	$\Delta S(\epsilon = 10)$ (cal/mol·K)
tyrosine−H_2O	−5.45	−28.2	−5.47	−24.4	−6.11	−31.7
histidine−H_2O	−5.68	−39.1	−6.73	−33.2	−6.94	−33.4

Hence, the motion of either water molecule required breaking of a hydrogen bond followed by the formation of a Mn(II)−water bond and possibly the displacement of the other ligands to accommodate the new sixth ligand. To obtain estimates of the relevant hydrogen-bonding energies, quantum chemical calculations were carried out on two model systems that resembled the tyrosine− and histidine−water hydrogen-bonded complexes. The former was modeled as a water/*p*-cresol pair and the latter as a water/3-(4-imidazole)propanamide pair (Figure 11). Geometry optimization and thermochemical analysis were carried out in the gas phase, as well as in a dielectric medium with a dielectric constant of either 4 or 10 D to take into account the protein environment. In the case of the tyrosine model, the geometry-optimized hydrogen-bond distance was no more than 0.1 Å longer than that observed in the crystal (pdb structure 1VEW),[42] depending on the dielectric constant used. In the case of the histidine model complex, the water molecule, in fact, made two hydrogen bonds: one to the imidazole ring and another to the carboxyl oxygen with the water oxygen equidistant to the two acceptors (3.1 Å). This configuration closely matched the position in the crystallographic structure.[42] However, in the structure, the water was closer to the carbonyl by 0.3 Å, with an overall distance between the ring nitrogen and the carbonyl oxygen of 6.4 Å. The calculated enthalpy and entropy of the hydrogen-bond formation for these models are summarized in Table 2. What is striking is that the theoretical values, especially in the case of the tyrosine−water complex, closely match those that were obtained from the van't Hoff analysis shown in the inset of Figure 5. If our experiments do indeed measure the transfer of a water molecule from Tyr34 or His30 to the Mn(II) ion, then the total change in free energy due to Mn(II)−water bond formation and requisite change in geometry must be close to zero. A second implication of the calculations is that since the penta- to hexacoordination transition was not observed for the enzymatically inactive EcMn(Fe)SOD, the water molecule must either be absent or its hydrogen bonding is significantly modified so that the equilibrium entirely favors hydrogen bonding to the amino acid. The second possibility appeared unlikely in light of the quantum calculations since the optimal geometry should correspond to the strongest hydrogen bonding. Nonetheless, both types of structural modifications would change the structure of the access channel, of which the water molecule is a part, as well as potentially modify proton-transfer pathways that are known to be important to enzyme activity.[8,9]

The octahedral structure that results from the addition of a water molecule to the normal pentacoordinated center would be structurally similar to that of the azide-bound MnSOD[25] and those seen by crystallography for the EcMnSOD protein under cryo-trapping conditions[41] and at high pH conditions in the ferric form of the cambialistic form of the *P. shermanii* SOD.[46] In the latter two cases, a water or hydroxide molecule was thought to be the sixth ligand. The cryo-trapped hexacoordinate EcMnSOD state must be different from the one that we observe since in our case, the hexacoordinate form existed in an equilibrium with the pentacoordinate form and at low temperatures required very long times to form. We attempted to characterize the cryo-trapped six-coordinate center. However, using conditions nearly identical to those of the single-crystal experiments, we were unable to trap any six-coordinate Mn(II) centers. This may have been due to the fact the single crystals were much smaller than our 0.6 cm^3 samples and could be cooled much faster. Another possibility was that the cryo-trapped species corresponded to only Mn(III) centers. This would be consistent with the known heterogeneous redox nature of the metal ion[41,47,48] and the 30% occupancy observed in the cryo-trapping experiments.[41]

The thermodynamic parameters for the five- to six-coordination conversion that we have measured are nearly identical to those reported for EcMn(III)SOD in the presence of azide[26] and are slightly lower than those for coordination changes observed in Fe(II)SOD from *Methanobacterium thermoautotrophicum*.[49] In the former, it has recently been shown that the sixth ligand of the hexacoordinate form is, in fact, an azide ion which exists in an equilibrium as the sixth ligand of the Mn(III) ion and also a hydrogen-bonded partner to the Tyr34.[50] In the *M. thermoautotrophicum* Fe(II)SOD, the transition occurred above freezing and may correspond to our observations above 268 K. It is surprising that the enthalpies and entropies for all three of these processes are so similar. This would support the notion that the driving force for these transitions resides in the protein, such as in hydrogen bonds, rather than in the metal−ligand interactions. Such nonmetal interactions are likely to play an important role in the function of Mn/Fe superoxide dismutases.

The observed temperature dependence of the MnSOD spectra also has important implications on the nature of the zero-field interaction of Mn(II) ions. The relationship between the symmetry of the hexacoordinate Mn(II) and the magnitude of $|D|$ was striking. Of course, the superposition model describes such a relationship. The existing data along with those we present here indicate that it is also true for complexes for which the SP model does not work, for example, the manganese-containing photosynthetic reaction centers and also the Mn(II)-doped bis(2-pyridylmethyl)amine complexes of Zn(II) and Cd(II). The Mn(II) sites in the latter cadmium complex have a relatively large $|D|$ value of 5.25 GHz (0.175 cm^{-1}), although the metal ion is bonded to six nitrogens all nearly at the same distance of 2.35 ± 0.02 Å. The asymmetry in this case resides purely in the angular orientation of the ligands. It appears that the SP

(44) Sharma, R. R.; Das, T. P.; Orbach, R. *Phys. Rev.* **1966**, *149*, 257−269.
(45) Sharma, R. R.; Das, T. P.; Orbach, R. *Phys. Rev.* **1967**, *171*, 338−352.
(46) Schmidt, M. *Eur. J. Biochem.* **1999**, *262*.
(47) Fee, J. A.; Shapiro, E. R.; Moss, T. H. *J. Biol. Chem.* **1976**, *251*, 6157−6159.
(48) Whittaker, M. M.; Whittaker, J. W. *J. Am. Chem. Soc.* **1991**, *113*, 5528−5540.
(49) Renault, J. P.; Morgenstern-Badarau, I.; Piccioli, M. *Inorg. Chem.* **1999**, *38*, 614−615.
(50) Jackson, T. A.; Karapetan, A.; Miller, A.-F.; Brunold, T. C. *J. Am. Chem. Soc.* **2004**, *126*, 12477−12491.

model is unable to handle such highly asymmetric cases. This suggests that the underlying mechanism(s) for the Mn(II) zero-field interaction in near octahedral and tetrahedral coordination geometries, which the SPM is able to empirically model so well, is not the same when there is significant asymmetry. Moreover, if the cryogenic temperature behavior of the zero-field interaction in the pentacoordinate Mn(II) ions in SODs is due to structural strain, then the implied distance dependence of $\sim r^{-2.5}$ suggests that the underlying mechanism for the zero-field interaction in these ions must also be different for the more symmetric hexa- and tetracoordinate systems. The most likely mechanism for the pentacoordinate and asymmetric hexacoordinate Mn(II) centers is the second-order spin−orbit contribution, which in the more symmetric hexa- and tetracoordinate ions is very small.[31,44,45] Both ab initio and semiempirical approaches are being pursued to clarify these issues.

Acknowledgment. We thank Guillaume Voyard for technical assistance. L.C.T. and N.C. acknowledge the support of CONICET, SeTCIP, and ANPCyT (PICT-8753 and PICT-5105) from Argentina, and the ECOS Sud/SeCyT collaboration program (Project A02B01).

Supporting Information Available: Tables of D and *E* values for EcMnSOD and Mn(Fe)SOD as a function of temperature. This material is available free of charge via the Internet at http://pubs.acs.org.

JA047007R